Atmos. Meas. Tech. Discuss., 5, 2043–2075, 2012
www.atmos-meas-tech-discuss.net/5/2043/2012/
doi:10.5194/amtd-5-2043-2012

Atmospheric Measurement Techniques Discussions

Quantification and mitigation of the impact of scene inhomogeneity on Sentinel-4 UVN UV-VIS retrievals

S. Noël[1], K. Bramstedt[1], H. Bovensmann[1], J. P. Burrows[1], C. Standfuss[2], E. Dufour[2], and B. Veihelmann[3]

[1]Institute of Environmental Physics, University of Bremen, FB 1, P.O. Box 330440, 28334 Bremen, Germany
[2]Noveltis, Parc Technologique du Canal, 2, avenue de l'Europe, 31520 Ramonville-St Agne, France
[3]ESA/ESTEC, Keplerlaan 1, 2201 AZ Noordwijk, The Netherlands

Received: 10 February 2012 – Accepted: 25 February 2012 – Published: 1 March 2012

Correspondence to: S. Noël (stefan.noel@iup.physik.uni-bremen.de)

Published by Copernicus Publications on behalf of the European Geosciences Union.

Abstract

The quality of trace gas products derived from measurements of a space-borne imaging spectrometer is affected by the inhomogeneity of the illumination of the instrument slit and thus by the heterogeneity of the observed scene. This paper aims to quantify this effect and summarise findings on how to mitigate the impact of inhomogeneous slit illumination on tropospheric O_3, NO_2, SO_2 and HCHO columns derived from measurements of the Sentinel-4 UVN imaging spectrometer. For this purpose, spectra for inhomogeneous ground scenes have been simulated based on a combination of a radiative transfer model and spatially high resolved MODIS (Moderate Resolution Imaging Spectroradiometer) data. The resulting errors on tropospheric O_3, NO_2, SO_2 and HCHO columns derived from these spectra have been determined via an optimal estimation approach. It could be concluded that inhomogeneous illumination results in significant errors in the data products if the natural inhomogeneity of the observed scenes is not accounted for. O_3 columns are less affected than the other data products; largest errors occur for NO_2 (mean absolute errors about 5 %, maximum error exceeding 50 %). These errors may be significantly reduced (by factors up to >10) by an appropriate wavelength calibration applied individually to each Earthshine radiance spectrum. With wavelength calibration the estimated mean absolute errors due to inhomogeneity are for all gases well below 1 %; maximum errors are about 10 % for NO_2 and around 5 % for the other gases.

1 Introduction

Light entering an imaging spectrometer is spectrally dispersed along one of the spatial dimensions of the scene that is seen through the telescope. Depending on the heterogeneity of the observed scene, the entrance slit of the spectrometer will be inhomogeneously illuminated, which results in a scene dependent slit function. This variable slit function, if not taken properly into account, will affect the spectral calibration of

AMTD
5, 2043–2075, 2012

the sensor (Voors et al., 2006) and will introduce a pseudo noise component into the measured top-of-the atmosphere reflectance (Earth radiance over solar irradiance). This pseudo-noise will then affect the quality of trace gas products derived from the reflectance spectra using absorption spectroscopic techniques like for example the Differential Optical Absorption Spectroscopy (DOAS, see e.g. Perner and Platt, 1979; Burrows et al., 1999), as these techniques ask for reflectance spectra with high signal-to-noise ratios.

Voors et al. (2006) investigated the impact of scene inhomogeneity, mainly due to clouds, on the spectral calibration of the Ozone Monitoring Instrument (OMI) on Aura (Levelt et al., 2006), which has a spatial resolution of up to $13 \times 24\,km^2$ (for the nadir pixels). They showed that inhomogeneous slit filling due to inhomogeneous scenes (clouds, etc.) results in wavelength shifts of the order of 0.01 nm. They concluded that with an adequate spectral calibration approach the impact of the inhomogeneous slit illumination on spectral calibration can be minimised. Gerilowski et al. (2011) demonstrated with an airborne spectrometer that scene inhomogeneities on scales smaller than 50 m result in enhanced noise contributions even under cloud free conditions. Nevertheless, there is to the authors knowledge no analysis of impact of scene inhomogeneity on the trace gas concentrations errors published so far. Therefore, this paper aims to quantify the impact and summarise findings on how to mitigate the impact of inhomogeneous slit illumination on trace gas concentrations. Specifically, the present study concentrates on measurements of weak absorbers in the UV-VIS spectral region performed by the Sentinel-4 UVN instrument.

The Sentinel-4 UVN instrument (Bazalgette Courrèges-Lacoste et al., 2011) is an imaging spectrometer designed to monitor air quality over Europe from geostationary orbit. The main purpose of the UVN mission is to monitoring the air quality by measurements of tropospheric O_3, NO_2, SO_2, HCHO and aerosol quantities. UVN is currently under development. The Sentinel-4 mission will consist of two instruments, the first one to be launched in 2018 on board MTG-S1. Similar to OMI, UVN will use 2-dimensional CCD detectors to measure direct as well as backscattered solar irradiance

AMTD
5, 2043–2075, 2012

in two spectral bands, the UV-VIS (305–500 nm, spectral resolution 0.5 nm) and the NIR (750–775 nm, spectral resolution 0.12 nm). The long side of the instrument slit is oriented in N-S direction. Continuous scans in E-W direction are performed to obtain a spectrally resolved image of Europe on an hourly scale.

The typical UVN ground pixel size is 8 km × 8 km. The natural heterogeneity of such a ground scene (due to e.g. different surface albedo or cloudiness) results in an inhomogeneous illumination of the instrument slit, which in turn alters the Instrument Spectral Response Function (ISRF). Since this ISRF depends on the actual scene, it is highly variable and usually not known (although there are possibilities to infer this ISRF from spatially higher resolved measurements). Effectively, the inhomogeneous illumination generates an additional error if it is not accounted for in the retrieval, i.e. if in the retrieval a homogeneous illumination is assumed.

This manuscript describes investigations performed to assess and mitigate the impact of inhomogeneous illumination of the instrument slit on the Sentinel-4 UVN UV-VIS data products O_3, NO_2, SO_2 and HCHO. Although the simulations shown in this manuscript have been specifically performed for the UVN instrumental configuration, the problem of inhomogeneous illumination and thus also possible mitigation strategies are also relevant for other missions using similar instrumentation, like the forthcoming Sentinel-5 and its precursor (with the TROPOMI instrument).

2 Approach

The overall approach to determine the errors of the tropospheric columns is as follows:

1. Compute a spectrally high resolved reference radiance using a radiative transfer model.

2. Simulate measured radiances for inhomogeneous scenes by convolution of the reference radiance with simulated inhomogeneous ISRFs, i.e. ISRFs derived for a heterogeneous scene as described below.

AMTD
5, 2043–2075, 2012

3. Simulate a measured irradiance by convolution of a reference irradiance spectrum with the corresponding homogeneous ISRF, i.e. an ISRF for homogeneous illumination.

4. (Optionally) apply a wavelength calibration.

5. Calculate the reflectance.

6. Estimate systematic errors of data products assuming a retrieval with homogeneous ISRF.

Steps 2 to 6 are performed for a set of 400 UVN ground pixels covering an area of 160 km × 160 km.

The following subsections summarise the input quantities and specific algorithms used in this study. More detailed information is given in the Appendix.

2.1 Radiance and irradiance spectra

The spectrum of Dobber et al. (2008) is used as irradiance reference spectrum. The radiance reference spectrum is derived by radiative transfer calculations using SCIATRAN 2.2 (Rozanov et al., 2005).

The following geophysical scenario has been assumed: Satellite position 0° N, 0° E, 35 786 km height, 23 September, 15:00 LT, latitude 50° N, surface albedo 0.05 (spectrally constant). The assumed aerosol settings and columns of trace gases are given in Tables 1 and 2. The tropospheric ozone column corresponds to typical background conditions; for the minor trace gases polluted conditions are assumed. This scenario is considered to be typical for the most interesting UVN measurement conditions. In fact, it is in line with the scenario used in the UVN signal-to-noise specifications. Note that the results presented in this study do not depend much on the chosen scenario as long as this scenario is consistently used in both forward model and retrieval.

AMTD
5, 2043–2075, 2012

2.2 Calculation of ISRFs

Simulated ISRFs for homogeneous and inhomogeneous scenes have been derived based on MODIS (Moderate Resolution Imaging Spectroradiometer, see http://modis.gsfc.nasa.gov) data. For this study, MODIS/Terra data from spectral band 3 (459–479 nm) have been used. In this band, MODIS data have a spatial sampling of 0.5 km which is considerably higher than the UVN spatial sampling of 8 km and thus allows the estimation of intensity variations over the UVN slit.

The method to derive these ISRFs is explained in Appendix A.

For the results presented in this manuscript a typical MODIS scene over land (relatively clear region over Spain, 17 June 2009) has been selected. This scene has been chosen because it contains many cloud-free ground pixels (providing the best situation to derive useful tropospheric information), but also pixels with higher cloud fraction, adding some more variability in the signal (see Fig. 1). The scene covers an area of 160 km × 160 km, which corresponds to 400 (20 × 20) UVN ground pixels.[1] This number is considered to be sufficient to derive statistically meaningful results.

In the context of this study the so-called "reflectance ratio" (RR) is used to characterise the inhomogeneity of a scene. The reflectance ratio is defined as:

$$\mathrm{RR} = \frac{L_{\mathrm{left}}}{L_{\mathrm{right}}} \tag{1}$$

where L_{left} denotes the sum of all sub-pixel reflectances left of the centre of the field of view/slit and L_{right} is the sum of all sub-pixel reflectances right of the centre. The reflectance ratio is determined from sub-pixel reflectance data also derived from MODIS.

[1]The Sentinel-4 spatial sampling distance (SSD) has been assumed constant (8 km) for simplicity. Variations of the SSD e.g. due to the projection on the Earth's surface have been ignored. The assumed SSD of 8 km is in line with the requirement at a reference location at 45° N.

AMTD
5, 2043–2075, 2012

Figure 2 shows the spatial distribution of the cloud fraction for the selected scene as well as the mean and standard deviation of the sub-pixel reflectances and the derived reflectance ratios. The cloud fraction is approximated by the reflectance variation between clear-sky and overcast threshold values derived empirically such that the average cloud fraction is consistent with the MODIS cloud cover product (at 5 km sampling) over the entire scene. Therefore, the spatial distribution of cloud fraction and reflectance is fully correlated. As expected, mean and standard deviation of the radiances typically correlate well with the cloud fraction; the reflectance ratio deviation from one is usually high at large cloud or reflectance gradients.

The reflectance ratio is also useful to classify the derived inhomogeneous ISRFs, as can be seen from Fig. 3. ISRFs with a reflectance ration close to 1 are symmetric and very similar to the homogeneous ISRF. The ISRFs become more asymmetric when the reflectance ratio deviates from 1.

2.3 Spectral calibration algorithm

The spectral calibration has been performed using a newly developed algorithm which is described in detail in Appendix B. The reference spectra used in the spectral calibration have been convoluted with the homogeneous ISRF. The spectral calibration algorithm uses as weights errors which have been derived from expected UVN signal-to-noise ratios (SNRs) shown in Fig. 4.

The spectral calibration algorithm used here differs in some respect from the one used in OMI operational processing (Voors et al., 2006). For OMI, the spectral calibration is performed in several steps: First, the wavelength calibration is determined for a number of irradiance spectra obtained at a reference temperature of the optical bench. This is done by fitting a reference solar spectrum to the measured irradiances. The second step is to estimate the spectral calibration for the actual optical bench temperature based on temperature dependencies determined pre-flight. Finally, to take into account the heterogeneity of the observed scene, an additional correction is applied to the measured radiances based on the knowledge of sub-pixel radiances.

AMTD
5, 2043–2075, 2012

The spectral calibration algorithm used in the present study is in fact very similar to the one performed during the first step of OMI wavelength calibration in the sense that in both cases absorption features are fitted to the measured spectra. However, in the present case the spectral calibration fit is applied to each individual radiance and irradiance spectrum without sub-pixel knowledge instead of using a-posteriori corrections.

2.4 Reflectance calculation algorithm

The UVN instrument will measure the spectral radiance R and the spectral irradiance I as functions of wavelength λ. The reflectance L is defined as the ratio of radiance to irradiance[2]:

$$L := \frac{R}{I}. \tag{2}$$

The problem is, that radiance and irradiance are usually measured on slightly different wavelength grids. Therefore, an interpolation is required. As the variability of irradiances is smaller than the variability of radiances, the preferred way is to interpolate the irradiance to the radiance spectral grid.

Different methods can be used for the interpolation. The simplest way is to perform a linear interpolation, but this may cause errors, if the spectra are not strongly oversampled (which is not the case for UVN spectra, where the sampling ratio is typically 3). A better method, which is quite commonly used also for spectral data from other instruments, is a spline interpolation.

In the present case we use the so-called "high sampling interpolation method" (further on abbreviated with HSM), which has been developed by Pepijn Veefkind from KNMI (personal communication, 2010).

[2]Note that other definitions of the reflectance exist, which include additional geometrical factors, like the cosine of the solar zenith angle. This is however not relevant in the context of this study, because these factors do not have a spectral dependence.

AMTD
5, 2043–2075, 2012

The HSM uses additional information from a solar reference spectrum with high sampling (I_{ref}). For the HSM, the irradiance at a spectral position λ_j is given by:

$$I(\lambda_j) = I(\lambda_k) \frac{I_{ref}(\lambda_j)}{I_{ref}(\lambda_k)} \quad (3)$$

where λ_k is the nearest neighbour spectral sample of λ_j and I_{ref} is linearly interpolated to λ_k and λ_j. A linear interpolation is sufficient in this case because of the high sampling of I_{ref}. Various tests have shown that for the UVN instrument the HSM method results – at least in the UV-VIS – in the smallest errors when applying a retrieval to the reflectances.

If the impact of the inhomogeneous slit illumination on the spectral calibration is not taken into account, this results in a spectral mismatch between the radiance and the irradiance spectrum which adds "pseudo noise" into the reflectance spectrum L. The introduced pseudo noise is in the order of a few tenth of a percent in the UV-VIS, which needs to be compared to the SNR requirements of this sensor type which is typically several 100 in the UV and several 1000 in the visible spectral range. Depending on the amplitude and the spectral correlation of that pseudo-noise, trace gas retrieval of weak absorbers might be degraded. Therefore in the next step the impact of inhomogeneous slit illumination on trace gas retrieval as well as options to minimise the impact will be assessed.

2.5 Error mapping

For the information content and error analysis approach an Optimal Estimation retrieval scheme and performance assessment (see e.g. Rodgers, 2000) using a-priori constraints for all relevant parameters assuming a linear or moderately linear problem (i.e. neglecting non-linearities) has been chosen. Details on this approach are given in Appendix C.

In the retrieval model, four trace gases are retrieved: O_3 (fitting window 305–330 nm), NO_2 (405–500 nm), SO_2 (308–325 nm), and HCHO (337–360 nm). For all quantities,

AMTD
5, 2043–2075, 2012

the profiles of the scenario as specified in Tables 1 and 2 are used as a-priori with an associated error of 50 %.

Note that it is assumed in the analysis, that the atmospheric state is perfectly known for all parameters except the retrieved one. Therefore, a small error for a geophysical parameter due to a single instrumental error does not necessarily mean that this parameter can be retrieved with the estimated error, as a full error budget needs to be built up, also including errors introduced by the imperfect knowledge of e.g. cloudiness, surface albedo or aerosol loading.

3 Results

Figure 5 shows the correlation between the estimated systematic (relative) errors for O_3, NO_2, SO_2 and HCHO tropospheric columns resulting from inhomogeneous illumination to the cloud fraction (left panels) and to the reflectance ratio (right panels) without a correction (red marks) and after a spectral calibration has been applied to each individual radiance (green marks). Note that, as mentioned in Sect. 2.5, the estimated errors only consider the effect of the inhomogeneous illumination of the instrument slit on the measured spectrum.

As can be seen from this figure, high errors are generally observed at high cloud fractions. Without correction, there is a strong correlation between the reflectance ratio and the trace gas errors, which shows that the reflectance ratio is suitable for a characterisation of the inhomogeneity. With spectral calibration the errors and also the correlation between errors and reflectance ratio are significantly reduced.

To further quantify the results a statistical analysis of the errors has been performed. The following quantities are determined for each gas:

- The mean absolute relative error.
- The maximum absolute relative error.

AMTD
5, 2043–2075, 2012

– The standard deviation of the relative error.

– The correlation coefficient between the relative error and the reflectance ratio.

These quantities are determined for the full set of 400 spatial pixels and also for a reduced set containing only ground pixels with cloud fractions smaller than 20 %. The latter is more representative for a real UVN data set, because for ground pixels with too high cloud fraction no reliable tropospheric columns can be determined.

The results are shown in Fig. 6. Corresponding histograms of error distributions with and without wavelength calibration are shown in Fig. 7.

The distribution of errors is rather symmetric around zero before the correction and becomes much narrower (and sometimes slightly asymmetric) when the wavelength calibration is applied. After wavelength calibration there is usually a strong peak around zero error.

Without wavelength calibration mean systematic errors of up to about 6% are possible; maximum errors even exceed 50 % (in the case of NO_2). The errors for O_3 are generally smaller than for the other products. With wavelength calibration errors are largely reduced: Mean errors are ∼1 % or smaller, maximum errors ∼10 % or smaller. The standard deviation of the errors is usually slightly larger than the mean absolute error and largely reduced when wavelength calibration is switched on. As already noticed before, the correlation of errors with the reflectance ratio is large without wavelength calibration and reduced afterwards. This is an indication that inhomogeneity is mostly compensated by the wavelength calibration. The main effect of the inhomogeneous illumination is the asymmetric ISRF (see Fig. 3), which results in an effective wavelength shift. This effect is corrected by the wavelength calibration. The second effect, the different shape of the ISRF, seems to play a minor role.

In Table 3 the main results after wavelength calibration and for cloud fractions up to 20 % are summarised. In addition, an error reduction factor is given which is defined as the ratio of the tropospheric column error (or standard deviation) without corrections to the corresponding value after mitigation (i.e. wavelength calibration). The error

AMTD
5, 2043–2075, 2012

reduction factor is especially high (>10) for SO_2 and HCHO, where the retrievals are known to be very sensitive to spectral errors.

4 Conclusions

The impact of inhomogeneous illumination on Sentinel-4 UVN UV-VIS data products (O_3, NO_2, SO_2 and HCHO) has been estimated based on simulated scenes. From the results presented above the following conclusions can be drawn:

- Inhomogeneity results in significant tropospheric column errors if no wavelength calibration is performed.
- With (good) wavelength calibration the systematic error due to heterogeneous scenes is largely reduced.
- The reflectance ratio is a good measure to characterise inhomogeneous illumination.

The mean absolute errors after spectral calibration are in the order of a few percent, which is about the estimated accuracy of the linear error mapping method. Thus, a wavelength calibration (performed for each radiance spectrum) seems to be sufficient to compensate the impact of inhomogeneous illumination.

However, all results presented here are based on simulated data only. Therefore it is recommended to determine representative ISRFs for inhomogeneous illumination during the on-ground calibration of UVN and to repeat the analysis described in this manuscript with these ISRFs and real measurement data and retrievals. In case larger errors are derived when using real measurement data the retrievals could be further improved by taking into account in-flight information on scene inhomogeneity and inhomogeneous ISRFs. This information could be derived from the analysis of sub-pixel readouts obtained during the scan.

AMTD
5, 2043–2075, 2012

Appendix A

Derivation of inhomogeneous ISRFs

The derivation of ISRFs is based on a general model of the spectral response function (SRF) for a dispersive spectrometer concept. The spectral dispersion is assumed to be perfectly aligned with the across-slit dimension of the spectrometer. Thus, the SRF model is reduced to this only dimension, and we understand the Point Spread Function (PSF) hereafter as the along-slit integral of the two-dimensional spatial response. The across-slit dimension is labelled x in slit coordinates and X in object coordinates.

The following instrumental parameters are used in the calculations:

- The telescope PSF (PSF_{tel}) in slit coordinates.
- The spectrometer PSF (PSF_{sp}) in slit coordinates.
- The slit size $\Delta x_S = 45\,\mu m$.
- The slit size projection on Earth $\Delta X_S = 8\,km$.
- The spectral oversampling factor F_{OS} (= 3 in the UV-VIS).
- The spectral sampling step (= 1/6 nm in the UV-VIS).

Thus, the linear spectral dispersion factor with respect to the slit coordinates is approximated by $\Psi_\lambda = 0.5\,nm/45\,\mu m$ in the UV-VIS. Currently, the PSFs are assumed to be wavelength independent. In the calculations the UVN PSF data sets for 500 nm (provided by ESA) are used. Note that the instrumental values assumed here correspond to the status during phase B1 of the UVN project in 2010.

A1 Spectral response of a spatial subsample

In order to account for the heterogeneous radiance field in the object space, it is necessary to consider the spectral response of discrete spatial subsamples k in the

AMTD
5, 2043–2075, 2012

across-slit dimension. In practice the width of subsamples depends on the available information on illumination variation within a UVN spatial sample. In our case, the width ΔX_k in object space corresponds to the information derived from MODIS data at 500 m sampling. It is thus convenient to define the subsample width Δx_k in slit coordinates by multiplication of ΔX_k with the ratio between slit size and spatial sampling distance $\Delta x_s / \Delta X_s$.

In a scheme from the entrance slit to the spectral detector, the spectral subsample response SRF_k is obtained as follows:

1. The subsample top-hat function (in the following represented by the symbol $\prod$) of width Δx_k and centred on the subsample centre slit coordinate x_k is convoluted (denoted by operator $\otimes$) with the telescope PSF ($\mathrm{PSF}_{\mathrm{tel}}$). The result provides the normalised slit illumination in slit coordinates.

2. The normalised slit illumination of outer subsamples is partly out of the slit, this part is cut off by multiplication with a top-hat function of width Δx_s, yielding the normalised slit illumination by sub-sample k entering the spectrometer.

3. This illumination is convoluted with the spectrometer PSF ($\mathrm{PSF}_{\mathrm{sp}}$), which results in the monochromatic detector illumination.

4. Convolution with the top-hat function of detector width (exit slit) size $\Delta x_D = \Delta x_s / F_{OS}$ and subsequent conversion into spectral coordinates by application of the spectral dispersion factor Ψ_λ yields the spectral response of subsample k:

$$\mathrm{SRF}'_k(\lambda + \delta\lambda) = \left(\left[\left(\prod \left(\frac{x - x_k}{\Delta x_k} \right) \otimes \mathrm{PSF}_{\mathrm{tel}}(x) \right) \prod \left(\frac{x}{\Delta x_s} \right) \right] \otimes \mathrm{PSF}_{\mathrm{sp}}(x) \otimes \prod \left(\frac{x}{\Delta x_D} \right) \right) \left(\frac{\delta\lambda}{\Psi_\lambda} \right). \quad \text{(A1)}$$

AMTD
5, 2043–2075, 2012

Equation (A1) describes the spectral response of a slit sub-sample in case that the illumination of this subsample stays constant during the acquisition period. In a continuous scan mode, the object space is smeared by a scan motion distance ΔX_s. To compute subsample intensities (c.f. Eq. A4 below), the scan motion has to be taken into account by smearing the MODIS radiance field at 500 m sampling with a one-dimensional top-hat function of width ΔX_s. This solution is not optimum, because the smearing process has to be applied to each geophysical scene the SRF model is applied to. Alternatively and equivalently, spatial subsamples can be defined in the object space, and represented over the dwell period in continuously progressing slit coordinates. The convenience is that input radiances have not to be further processed. The scan motion is entirely (and once for all) taken into account by an additional convolution of sub-sample SRFs in slit coordinates with the motion smear function:

$$\mathrm{SRF}_k(\lambda + \delta\lambda) = \left(\left[\left(\left\{\prod\left(\frac{x}{\Delta x_s}\right) \otimes \prod\left(\frac{x - x_k}{\Delta x_k}\right)\right\} \otimes \mathrm{PSF}_{\mathrm{tel}}(x)\right)\prod\left(\frac{x}{\Delta x_s}\right)\right] \otimes \mathrm{PSF}_{\mathrm{sp}}(x) \otimes \prod\left(\frac{x}{\Delta x_D}\right)\right)\left(\frac{\delta\lambda}{\Psi_\lambda}\right). \quad \text{(A2)}$$

We apply Eq. (A2) as SRF model for subsamples of width 500 m in object space.

A2 Instrument spectral response function

The sum of all K non-zero subsamples SRF_k yields the total SRF in case of homogeneous slit illumination:

$$\mathrm{ISRF}^{\mathrm{hom}}(\lambda + \delta\lambda) = \sum_{k=1}^{K} \mathrm{SRF}_k(\lambda + \delta\lambda). \quad \text{(A3)}$$

For perfect optics, K would be 32 (slit size and smearing distance both correspond to 16 sub-samples or 8 km). However, there is an additional broadening due to the PSF which in the present case results in $K = 36$.

AMTD
5, 2043–2075, 2012

This function is independent of geophysically driven illumination conditions and can be referred to as the Instrument Spectral Response Function (ISRF). Without any mitigation attempts, this function would be considered in the level 2 processing together with the measured spectra.

Heterogeneous illumination conditions within a spatial sample will modify the shape of the actual spectral response with respect to the ISRF. With S_k being the intensity of sub-sample k (in object space), the actual total spectral response is given by:

$$\mathrm{ISRF}\,(\lambda + \delta\lambda) = \frac{\sum_{k=1}^{K} S_k\,\mathrm{SRF}_k\,(\lambda + \delta\lambda)}{\sum_{k=1}^{K} S_k}. \tag{A4}$$

The homogeneous ISRF of Eq. (A3) is therefore a special case of Eq. (A4) with equal weights S_k.

In Eqs. (A1)–(A4) the sub-sample SRFs and the ISRF come out in arbitrary units. We define these arbitrary units such that the ISRF fulfils the normalisation condition:

$$\int \mathrm{ISRF}\,(\lambda + \delta\lambda)\,\mathrm{d}(\delta\lambda) = 1. \tag{A5}$$

Appendix B

Spectral calibration algorithm

The originally foreseen spectral calibration algorithm for UVN was based on a peak finding routine similar to the one used in the SCIAMACHY project, which uses the Falk (1984) algorithm. However, first tests with simulated UVN data showed that the accuracy of this algorithm is not sufficient to fulfil the UVN spectral stability requirements. Therefore, an alternative algorithm for spectral calibration has been developed. This

AMTD
5, 2043–2075, 2012

algorithm has shown to work both in the UV-VIS and in the NIR, but in the context of the present manuscript only UV-VIS data are used.

The underlying assumptions for the algorithm are:

1. A first-guess wavelength calibration is available (e.g. from on-ground calibration) for the whole band, i.e. there should be an initial wavelength value associated to each spectral pixel.

2. The spectral variation of the wavelength calibration over the detector should be such that the "real" wavelength axis λ_R of S can be described as a low-order polynomial function $P_A(\lambda)$.

The main idea of the algorithm is to determine the coefficients of P_A by a non-linear least squares fit using the following equation:

$$y(\lambda) = P_B(\lambda) + y_{\text{ref}}(P_A(\lambda)) \tag{B1}$$

where

$$y := \ln(S) \tag{B2}$$

$$y_{\text{ref}} := \ln(S_{\text{ref}}). \tag{B3}$$

Here, S is a measured (irradiance or radiance) spectrum which is a function of wavelength λ, given of course at instrument spectral resolution and sampling. S_{ref} denotes a spectrally well-calibrated (radiance or irradiance) reference spectrum which is a function of the "true" wavelength λ_R. A potential broadband radiometric offset between S and S_{ref} is taken into account by the polynomial P_B. Fit parameters are the coefficients of the polynomials P_A and P_B. The resulting wavelength calibration is then given by:

$$\lambda_R = P_A(\lambda). \tag{B4}$$

The fit is performed for each UVN band (UV-VIS and NIR) independently, but for the whole band in one go. This directly results in a wavelength calibration for the complete band.

AMTD
5, 2043–2075, 2012

The algorithm as described above is suitable for the wavelength calibration of irradiance spectra. However, a major challenge of the spectral calibration of radiances is the large dynamic range of possible radiances, which depend e.g. on atmospheric absorption/scattering and surface albedo. As a consequence, there is a (wavelength dependent) intensity difference between the measured radiance (y) and the reference spectrum (y_{ref}), which usually can not be sufficiently compensated by the low order polynomial P_B.

The algorithm is able to handle these variabilities in the following ways, or by a combination of these:

1. By increasing the degree of the background polynomial P_B. Currently, a degree of 2 is used for irradiances and 12 for radiances.

2. By an additional fit of spectral absorber features (i.e. of ozone in the UV-VIS and O_2 in the NIR), denoted with α, which is defined as:

$$\alpha(\lambda) := \frac{\partial y_{\text{ref}}}{\partial c}\, c \tag{B5}$$

where c is the absorber amount (column) in absolute units and $\frac{\partial y_{\text{ref}}}{\partial c}$ is the absorber weighting function derived from radiative transfer calculations. Thus, α is essentially a normalised weighting function.

Considering α in the fit leads to the following slightly modified equation:

$$y(\lambda) = P_B(\lambda) + y_{\text{ref}}(P_A(\lambda)) + s\,\alpha(P_A(\lambda)) \tag{B6}$$

where s is a scaling factor which corresponds to a relative change of the absorber amount compared to the reference scenario. The usage of α in Eq. (B6) was inspired by the weighting function DOAS method (see e.g. Coldewey-Egbers et al., 2005). As y_{ref}, α is determined with SCIATRAN.

Another problem for the spectral calibration of radiances is that the intensities of the radiances decrease rapidly towards the UV due to ozone absorption. If also the

AMTD
5, 2043–2075, 2012

lower UV wavelengths are included in the fit, large uncertainties in the derived spectral calibration may occur. To reduce the impact of these wavelengths on the spectral calibration, the fit is performed using the error on the data as weights. Currently, this error is derived from signal-to-noise (see Fig. 4) only, but in-flight the end-to-end error could be used instead.

Appendix C

Error mapping approach

Here we describe in detail the analysis method to estimate the impact of systematic errors in the measured reflectances on the retrieved tropospheric trace gas columns. A quite general Bayesian/Optimal Estimation approach is used as described in more detail in (e.g. Rodgers, 2000). In the following we outline the error mapping approach in mathematical terms using a vector/matrix notation. The vector/matrix components correspond to:

- discrete wavelengths (mostly measurement detector pixel or channel centre wavelength)
- two altitude levels (troposphere, 0–10 km and stratosphere, 10–80 km).

Let $\boldsymbol{x}$ be the vector of parameter of interest (e.g. the discretised O_3 profile), $\boldsymbol{x}_a$, $\mathbf{S}_a$ be the corresponding a-priori information (parameter vector and covariance matrix) and $\boldsymbol{c}$ be the vector of other (assumed known) parameters (like atmospheric state/geolocation).

The high-resolution spectral reflectance $\boldsymbol{L}_{\text{high}}$ is computed via the radiative transfer model (RTM) F (at sufficiently high spectral and vertical resolution):

$$\boldsymbol{L}_{\text{high}} = F(\boldsymbol{x}, \boldsymbol{c}). \quad \text{(C1)}$$

AMTD
5, 2043–2075, 2012

The (logarithm of the) simulated measured spectral reflectance $\boldsymbol{y}$ is then derived using the instrument model M and a set of instrument parameters i_{m}:

$$\boldsymbol{y} = M\left(\boldsymbol{L}_{\mathrm{high}}, i_{\mathrm{m}}\right). \tag{C2}$$

The corresponding measurement error covariance matrix is denoted by $\mathbf{S}_y$. In the present case, the instrument model essentially contains the convolution of $\boldsymbol{L}_{\mathrm{high}}$ with the ISRF and the application of the instrument sampling.

The weighting function matrix $\mathbf{K}$ is defined as

$$\mathbf{K} := \frac{\mathrm{d}\boldsymbol{y}}{\mathrm{d}\boldsymbol{x}}. \tag{C3}$$

Note that the forward model computes the weighting functions on a 1 km altitude grid. The weighting functions are then summed up over the relevant tropospheric and stratospheric sub-columns.

The measured (logarithm of the) reflectance for the a-priori scenario $\boldsymbol{x}_{\mathrm{a}}$ is given by:

$$\boldsymbol{y}_{\mathrm{a}} = M(F(\boldsymbol{x}_{\mathrm{a}}, \boldsymbol{c}), i). \tag{C4}$$

Here, i denotes a set of instrument parameters assumed in the retrieval. This is not necessarily identical to the set i_{m} used in the calculation of the measured spectra. In the present case, different ISRFs are used in the calculation of $\boldsymbol{y}$ and $\boldsymbol{y}_{\mathrm{a}}$, namely inhomogeneous ISRFs for $\boldsymbol{y}$ and a homogeneous ISRF for $\boldsymbol{y}_{\mathrm{a}}$ (and also $\mathbf{K}$).

The measured (logarithm of the) reflectance for the actual scenario $\boldsymbol{x}$ is then approximated by:

$$\boldsymbol{y} \approx \boldsymbol{y}_{\mathrm{a}} + \mathbf{K}(\boldsymbol{x} - \boldsymbol{x}_{\mathrm{a}}). \tag{C5}$$

The solution vector (containing the retrieved parameters) is then given by

$$\hat{\boldsymbol{x}} = \boldsymbol{x}_{\mathrm{a}} + \mathbf{G}(\boldsymbol{y} - \boldsymbol{y}_{\mathrm{a}}) \tag{C6}$$

AMTD
5, 2043–2075, 2012

with the retrieval (gain) matrix

$$\mathbf{G} := \frac{\mathrm{d}\hat{\boldsymbol{x}}}{\mathrm{d}\boldsymbol{y}} = \mathbf{S}_{\hat{x}}\,\mathbf{K}^T\,\mathbf{S}_y^{-1} \tag{C7}$$

and the solution error covariance matrix

$$\mathbf{S}_{\hat{x}} = \left(\mathbf{K}^T\,\mathbf{S}_y^{-1}\,\mathbf{K} + \mathbf{S}_{\mathrm{a}}^{-1}\right)^{-1}. \tag{C8}$$

The systematic errors (in the present case those resulting from inhomogeneous illumination) are then given by the difference between the retrieved and true (a-priori) state vectors:

$$\Delta\hat{\boldsymbol{x}} = \boldsymbol{x} - \boldsymbol{x}_{\mathrm{a}} = \mathbf{G}(\boldsymbol{y} - \boldsymbol{y}_{\mathrm{a}}). \tag{C9}$$

The elements of $\Delta\hat{\boldsymbol{x}}$ are the errors of the tropospheric and stratospheric columns.

Note that for some combinations of retrieved parameters and assumed errors, a subtraction of a polynomial in the retrieval improves the results. This is a standard technique for retrievals on real data. In this case, the state vector $\boldsymbol{x}$ will contain additional entries (3 in case of a second order polynomial) which are the coefficients of the polynomial as additional fit parameters.

Acknowledgements. MODIS data have been retrieved from the Level 1 and Atmosphere Archive and Distribution System (LAADS). This work has been performed in the context of the "In-flight Spectral Calibration and Requirements on Reflectance for Sentinel-4" study, ESA ESTEC Contract 4000101187/10/NL/MP/ef.

AMTD
5, 2043–2075, 2012

References

Bazalgette Courrèges-Lacoste, G., Ahlers, B., Guldimann, B., Short, A., Veihelmann, B., and Stark, H.: The Sentinel-4/UVN instrument on-board MTG-S, in: Proc. of 2011 EUMETSAT Meteorological Satellite Conference, 5–9 September 2011, EUMETSAT P. 59, Oslo, Norway, 2011. 2045

Burrows, J. P., Weber, M., Buchwitz, M., Rozanov, V., Ladstätter-Weißenmayer, A., Richter, A., de Beek, R., Hoogen, R., Bramstedt, K., Eichmann, K.-U., Eisinger, M., and Perner, D.: The Global Ozone Monitoring Experiment (GOME): Mission Concept and First Scientific Results, J. Atmos. Sci., 56, 151–175, 1999. 2045

Coldewey-Egbers, M., Weber, M., Lamsal, L. N., de Beek, R., Buchwitz, M., and Burrows, J. P.: Total ozone retrieval from GOME UV spectral data using the weighting function DOAS approach, Atmos. Chem. Phys., 5, 1015–1025, doi:10.5194/acp-5-1015-2005, 2005. 2060

Dobber, M., Voors, R., Dirksen, R., Kleipool, Q., and Levelt, P.: The High-Resolution Solar Reference Spectrum between 250 and 550 nm and its Application to Measurements with the Ozone Monitoring Instrument, Sol. Phys., 249, 281–291, doi:10.1007/s11207-008-9187-7, 2008. 2047

Falk, W. R.: Data Reduction from Experimental Histograms, Nucl. Instrum. Meth. Phys. Res., 220, 473–478, 1984. 2058

Gerilowski, K., Tretner, A., Krings, T., Buchwitz, M., Bertagnolio, P. P., Belemezov, F., Erzinger, J., Burrows, J. P., and Bovensmann, H.: MAMAP – a new spectrometer system for column-averaged methane and carbon dioxide observations from aircraft: instrument description and performance analysis, Atmos. Meas. Tech., 4, 215–243, doi:10.5194/amt-4-215-2011, 2011. 2045

Levelt, P., van den Oord, G., Dobber, M., Malkki, A., Visser, H., de Vries, J., Stammes, P., Lundell, J., and Saari, H.: The ozone monitoring instrument, Geoscience and Remote Sensing, IEEE T. Geosci. Remote, 44, 1093–1101, doi:10.1109/TGRS.2006.872333, 2006. 2045

Perner, D. and Platt, U.: Detection of Nitrous Acid in the Atmosphere by Differential Optical Absorption, Geophys. Res. Lett., 6, 917–920, 1979. 2045

Rodgers, C. D.: Inverse Methods for Atmospheric Sounding: Theory and Practice, Series on Atmospheric, Oceanic and Planetary Physics, vol. 2, World Scientific Publishing Co. Pte. Ltd., Singapore, 2000. 2051, 2061

AMTD
5, 2043–2075, 2012

Rozanov, A., Rozanov, V., Buchwitz, M., Kokhanovsky, A., and Burrows, J. P.: SCIATRAN 2.0 – A new radiative transfer model for geophysical applications in the 175–2400 nm spectral region, Adv. Space Res., 36, 1015–1019, doi:10.1016/j.asr.2005.03.012, 2005. 2047

Voors, R., Dobber, M., Dirksen, R., and Levelt, P.: Method of calibration to correct for cloud-induced wavelength shifts in the Aura satellite's Ozone Monitoring Instrument, Appl. Optics, 45, 3652–3658, 2006. 2045, 2049

AMTD

5, 2043–2075, 2012

Table 1. Aerosol settings, based on Lowtran (moderate aerosol).

Season	Fall/Winter
Boundary layer aerosol type	Rural
Boundary layer visibility	23 km
Boundary layer humidity	80 %
Tropospheric visibility	23 km
Tropospheric humidity	80 %
Stratospheric aerosol loading	Background
Stratospheric aerosol type	Background
Mesospheric aerosol loading	Normal mesosphere

AMTD
5, 2043–2075, 2012

Table 2. Trace gases columns.

Trace Gas	Tropospheric Column (mol cm^{-2})	Total Column (mol cm^{-2})
O_3	6.4e+17	9.19e+18
NO_2	1.0e+16	1.58e+16
SO_2	9.1e+16	9.18e+16
HCHO	3.0e+16	3.10e+16

AMTD
5, 2043–2075, 2012

Table 3. Summary of results including wavelength calibration taking into account only ground pixels with maximum cloud fraction of 20 %.

O_3	No Correction	After Wavelength Cal.	Error Reduction
Mean absolute rel. error	1.2 %	0.3 %	4.4
Maximum absolute rel. error	10.8 %	4.7 %	2.3
Standard deviation of rel. errors	1.9 %	0.5 %	3.8
Correlation coefficient	−0.7	0.4	–
NO_2	No Correction	After Wavelength Cal.	Error Reduction
Mean absolute rel. error	5.2 %	0.8 %	6.6
Maximum absolute rel. error	54.2 %	11.1 %	4.9
Standard deviation of rel. errors	8.4 %	1.5 %	5.8
Correlation coefficient	0.7	0.3	–
SO_2	No Correction	After Wavelength Cal.	Error Reduction
Mean absolute rel. error	5.1 %	0.5 %	10.9
Maximum absolute rel. error	45.9 %	5.8 %	7.9
Standard deviation of rel. errors	8.1 %	0.7 %	12.0
Correlation coefficient	0.7	−0.6	–
HCHO	No Correction	After Wavelength Cal.	Error Reduction
Mean absolute rel. error	4.2 %	0.6 %	7.4
Maximum absolute rel. error	36.5 %	3.2 %	11.4
Standard deviation of rel. errors	6.7 %	0.8 %	8.4
Correlation coefficient	0.7	−0.2	–

AMTD
5, 2043–2075, 2012

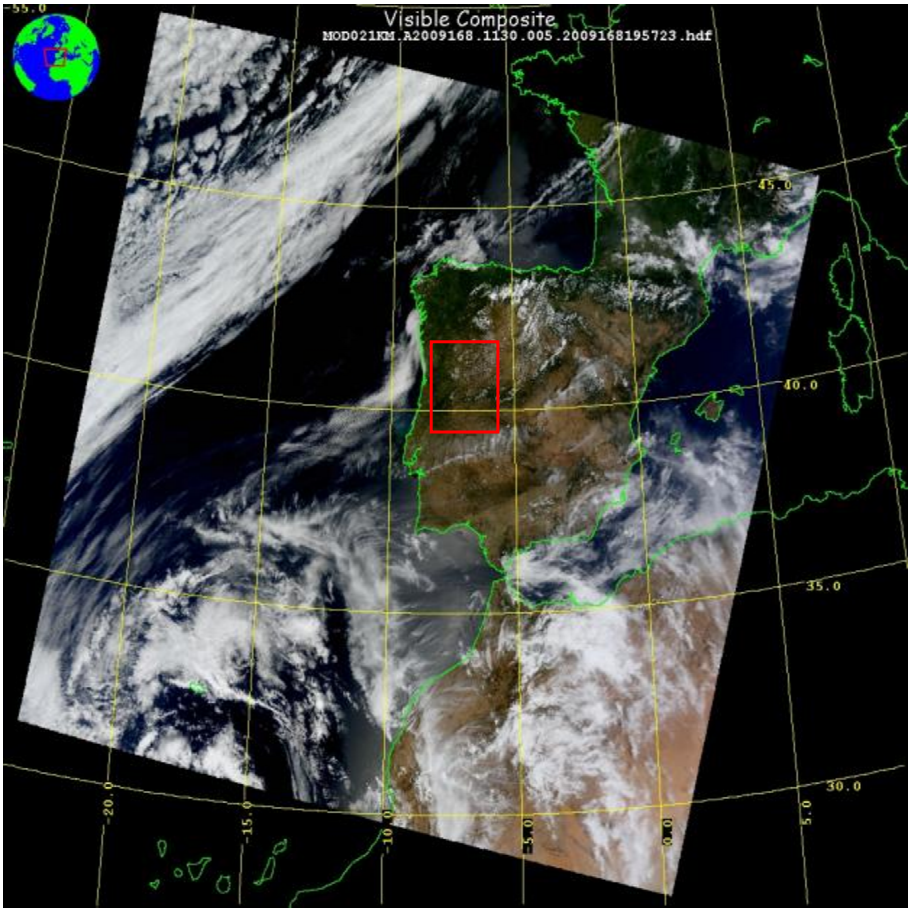

Fig. 1. Visible composite of MODIS/Terra data for 17 June 2009, 11:30–11:35 UT. Source: LAADS. The red square indicates the approximate position of the chosen region.

AMTD
5, 2043–2075, 2012

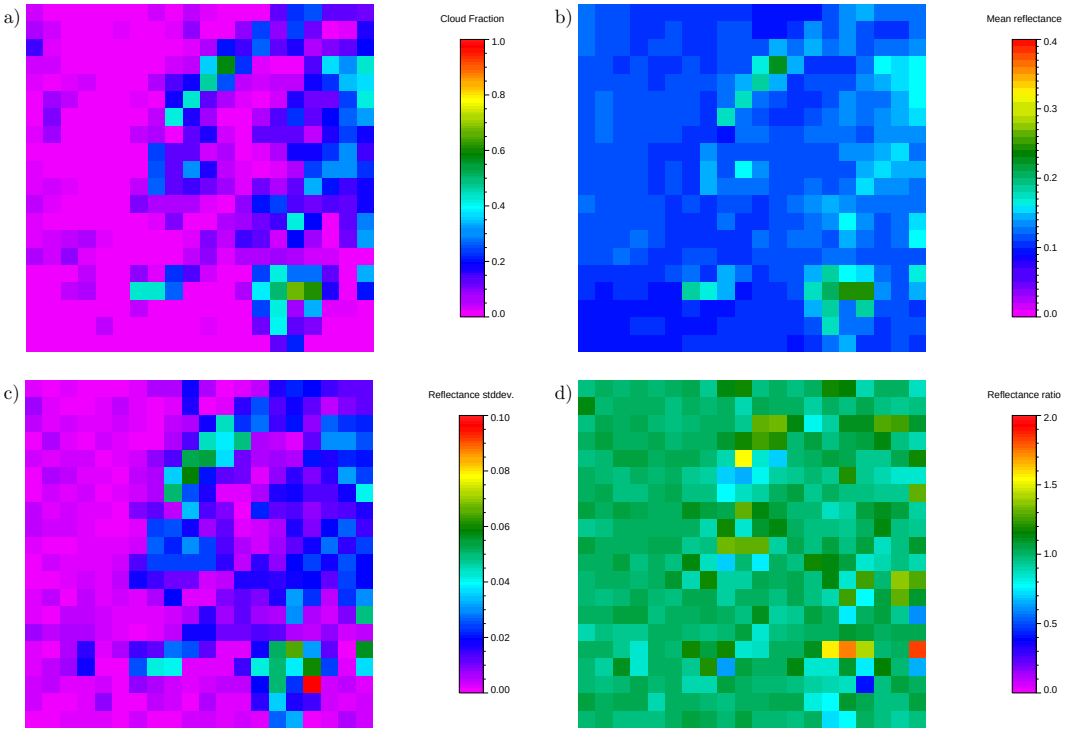

Fig. 2. Spatial distribution of reflectance quantities for the selected scene. Each square in the sub-figures correspond to one UVN ground pixel. **(a)** Cloud fraction, **(b)** mean sub-pixel reflectances, **(c)** standard deviation of sub-pixel reflectances, **(d)** reflectance ratios (as defined in Eq. 1).

AMTD
5, 2043–2075, 2012

Impact of scene inhomogeneity on UVN retrievals

S. Noël et al.

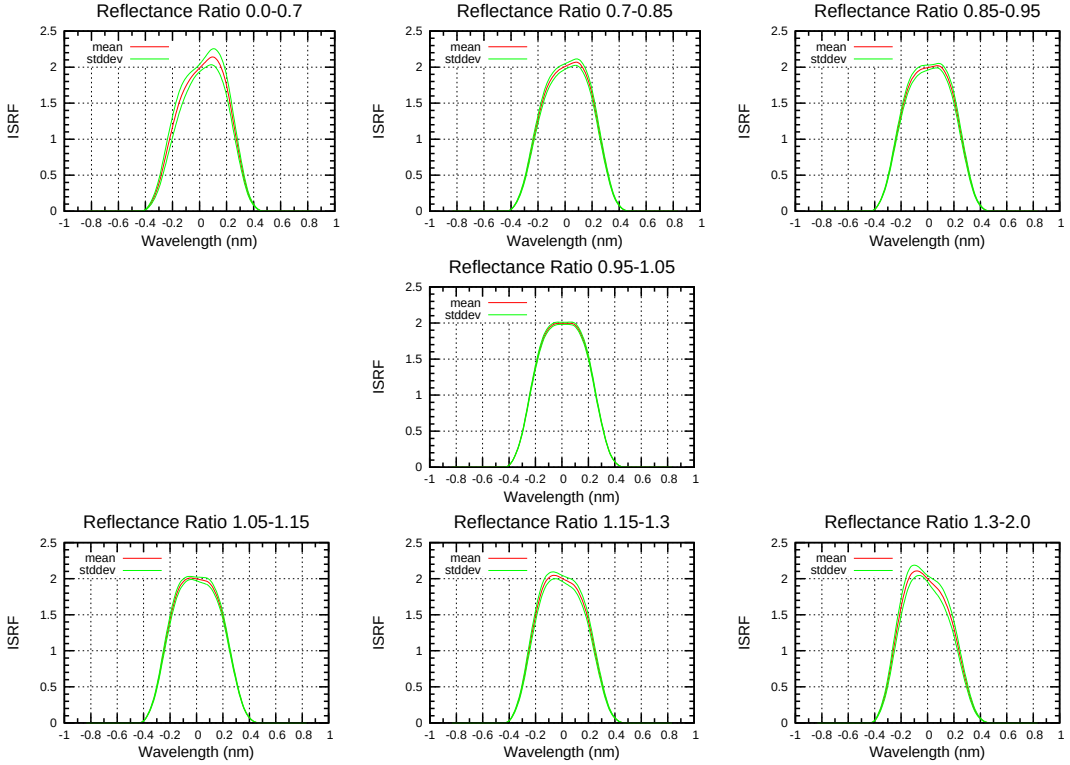

Fig. 3. Classification of inhomogeneous ISRFs. Red: mean ISRFs for the specified interval of reflectance ratios. Green: plus/minus corresponding standard deviation.

AMTD
5, 2043–2075, 2012

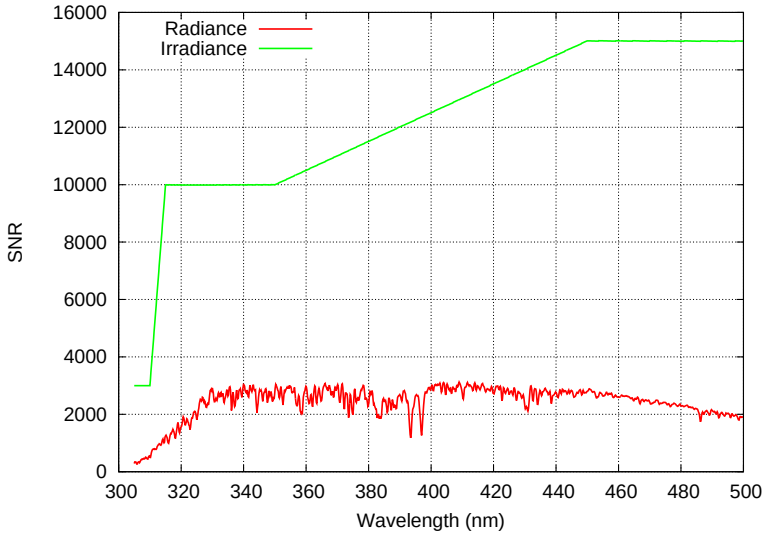

Fig. 4. Expected signal-to-noise ratios of the UVN instrument in the UV-VIS band. The irradiance SNR shown is the requirement.

AMTD
5, 2043–2075, 2012

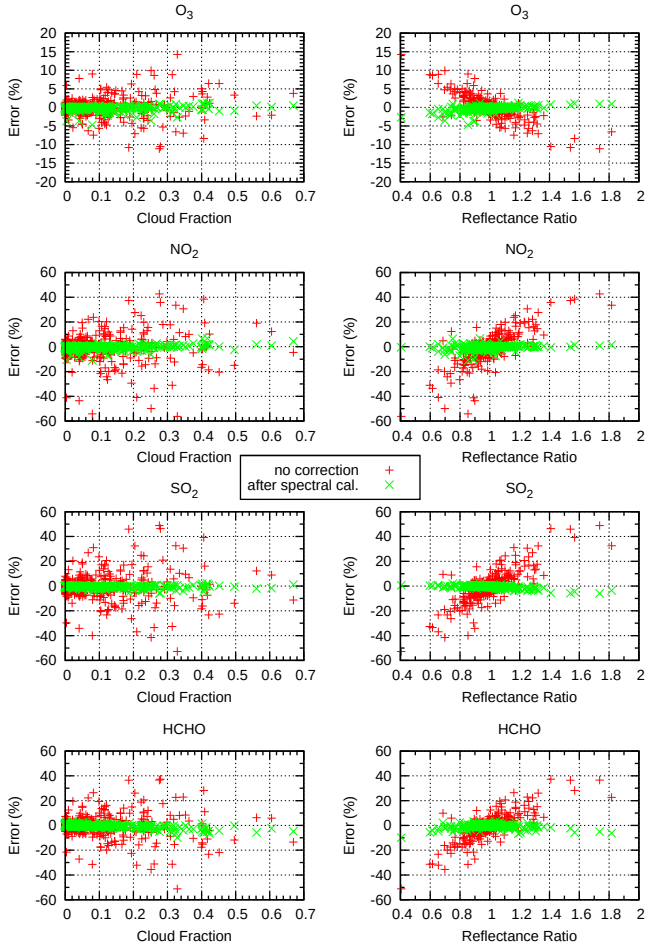

Fig. 5. Tropospheric column errors as function of cloud fraction (left panels) and reflectance ratio (right panels) without (red) and with (green) spectral calibration.

AMTD
5, 2043–2075, 2012

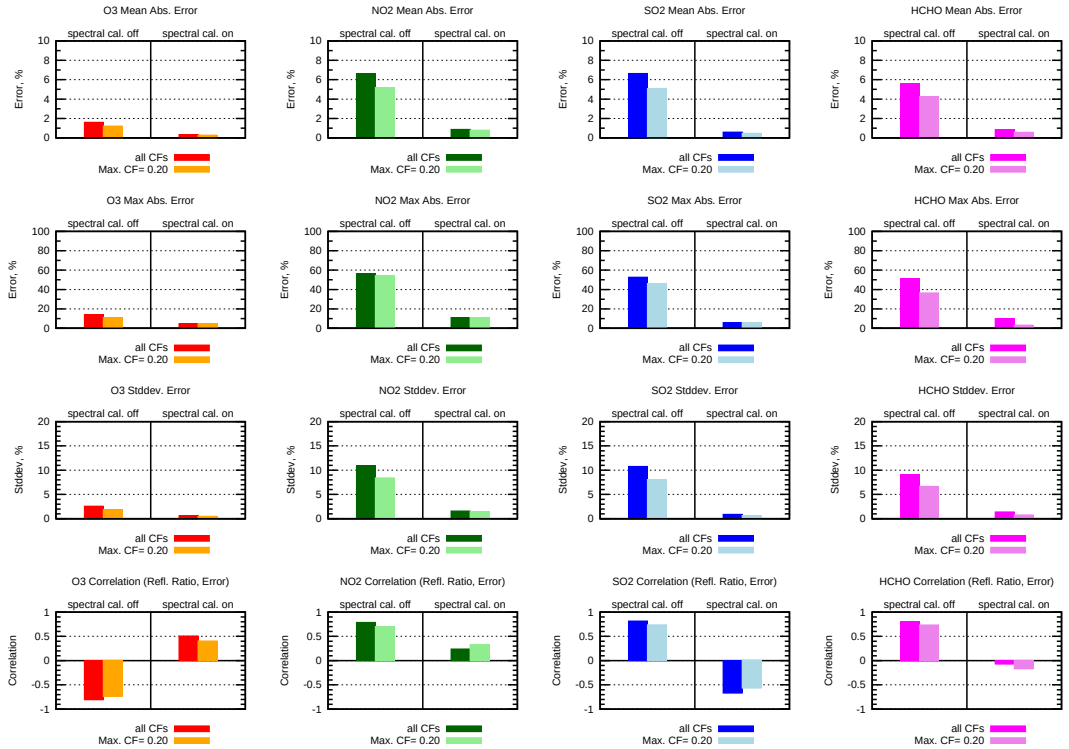

Fig. 6. Estimated errors of O_3 (red/orange), NO_2 (green), SO_2 (blue) and HCHO (magenta). Top row: Mean error, 2nd row: maximum error, 3rd row: standard deviation of error, bottom row: correlation with the reflectance ratio. Values are given with and without spectral calibration, and for different maximum cloud fractions (100 % and 20 %).

AMTD
5, 2043–2075, 2012

Impact of scene inhomogeneity on UVN retrievals

S. Noël et al.

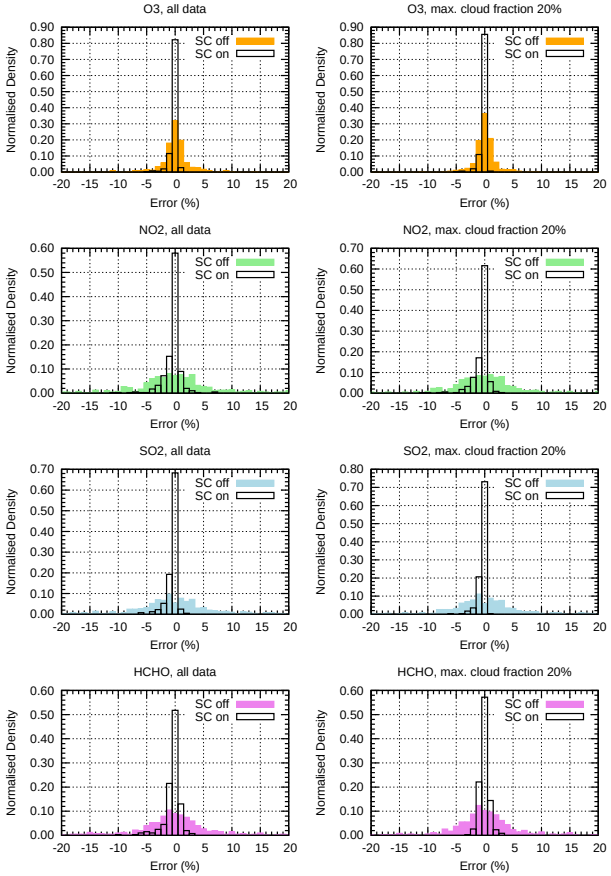

Fig. 7. Histograms of systematic errors due to scene inhomogeneity. The y-axis shows the number of sub-pixels with error in each bin (binsize 1 %), normalised to the total number of sub-pixels. Coloured boxes: without wavelength calibration, open boxes: with wavelength calibration, left panels: based on all data, right panels: based on only data with maximum cloud fraction of 20 %.

AMTD
5, 2043–2075, 2012